BIOCHEMISTRY
including biophysical chemistry & molecular biology
Article

Biochemistry **2010,** *49,* 10691–10701 10691
DOI: 10.1021/bi100580s

Probing the Structural Determinants for the Function of Intracellular Loop 2 in Structurally Cognate G-Protein-Coupled Receptors†

Jufang Shan,‡ Harel Weinstein,‡,§ and Ernest L. Mehler*,‡

‡*Department of Physiology and Biophysics and* §*The HRH Prince Alwaleed Bin Talal Bin Abdulaziz Alsaud Institute for Computational Biomedicine, Weill Cornell Medical College, Cornell University, New York, New York 10065, United States*

Received April 15, 2010; Revised Manuscript Received October 18, 2010

ABSTRACT: Intracellular loop 2 (*IL2*) in G-protein-coupled receptors (GPCRs) is functionally important, e.g., in binding to G-protein and β-arrestin. Differences in secondary structure of *IL2* in the crystal structures of the very similar β_1- and β_2-adrenergic receptors (β_1AR and β_2AR, respectively), i.e., an α-helix and an L-shaped strand, respectively, emphasize the need to understand the structural basis for *IL2* functionality. We studied the properties of *IL2* in the context of experimental data using a Monte Carlo-based *ab initio* method. The procedure was validated first by verifying that the *IL2* structures in β_1AR and β_2AR crystals were correctly reproduced, even after conformational ensemble searches at >1200 K where most secondary structure had been lost. We found that *IL2* in β_1AR and β_2AR sampled each other's conformation but adopted different energetically preferred conformations, consistent with the crystal structures. The results indicate a persistent contextual preference for the structure of *IL2*, which was conserved when the *IL2* sequences were interchanged between the receptors. We conclude that the protein environment, more than the *IL2* sequence, regulates the *IL2* structures. We extended the approach to the molecular model of 5-HT_{2A}R for which no crystal structure is available and found that *IL2* is predominantly helical, similar to *IL2* in β_1AR. Because the P3.57A mutation in *IL2* had been shown to decrease β-arrestin binding and internalization, we predicted the effects of the mutation and found that it decreased the propensity of *IL2* to form helix, identifying the helical *IL2* as a component of the GPCR active form.

G-Protein-coupled receptors (GPCRs)[1] are membrane proteins with highly dynamic structures that access many conformational states related to their functional mechanisms as well as to a biologically important functional plasticity, such as the ability to respond differentially to different ligands (*1*, *2*). Not surprisingly, the function-related structural flexibility is particularly pronounced in some of the loops, as demonstrated for the second extracellular loop, the second intracellular loop (*IL2*), and the third intracellular loop (*3*−*10*). In particular, there is also substantial evidence in the literature for the involvement of two specific residues in the observed functional actions of *IL2*, at positions 3.57 and 3.58 [Ballesteros−Weinstein numbering (*11*)], where mutations were shown to affect G-protein activation, binding to β-arrestin, and β-arrestin-mediated internalization (*12*−*15*). Both loci are highly conserved in class A GPCR (position 3.57, 64% Pro and 26% Ala; position 3.58, mostly bulky and hydrophobic with 75% of GPCRs having Ile/Leu/Val/Phe) (*14*). The P3.57A (Pro3.57 mutated to Ala) mutation in human muscarinic cholinergic receptor 1 or 3 (Hm1 or Hm3, respectively) inhibits phosphatidylinositol turnover, and substitution of Pro3.57 with polar residues such as Asp or Asn in Hm1 results in defective coupling (*13*). P3.57A in the β_2-adrenergic receptor (β_2AR) and serotonin 2C receptor (5-HT_{2C}R) decreases β-arrestin binding and β-arrestin-mediated internalization, whereas the inverse mutation A3.57P in α_{2A}-adrenergic receptor (α_{2A}AR) and neuropeptide Y type 2 receptor (NPY2R) increases internalization (*14*). Mutating Pro3.57 or Met3.58 to Ala in rhodopsin reduces R175E-arrestin binding (*12*). In the 5-HT_{2C}R, RNA editing that changes the INI sequence (Ile3.54-Asn3.56-Ile3.58) to VGV causes significant structural changes in the loop and its interaction with G-protein (*16*, *17*), and these lead to significant changes in both pharmacological and physiological properties (*18*, *19*). All these observations suggest that the highly conserved proline/alanine at position 3.57 is a key determinant of *IL2* function and that it determines the probability of transition between its active and inactive form. In the present study we identify the structural characteristics and identify the determinants for differences in propensity for the two forms in the structurally similar GPCRs.

Experimental data show that *IL2* can adopt both helical and nonhelical conformational states, under different conditions. It was suggested that *IL2* is helical in m5 muscarinic receptor and is a determinant for G-protein coupling (*3*). In the angiotensin II (AT1A) receptor *IL2* does not have a defined secondary structure

†The work was supported by National Institutes of Health grants from the National Institute on Drug Abuse (P01 DA012923 and R01 DA015170).

*To whom correspondence should be addressed. E-mail: elm2020@med.cornell.edu. Phone: (212) 746-6365. Fax: (212) 746-8690.

[1]Abbreviations: *IL2*, intracellular loop 2; GPCRs, G-protein-coupled receptors; β_1AR, β_1-adrenergic receptor; β_2AR, β_2-adrenergic receptor; P3.57A, Pro3.57 mutated to Ala; Hm1, human muscarinic cholinergic receptor 1; Hm3, human muscarinic cholinergic receptor 3; 5-HT_{2C}R, serotonin 2C receptor; α_{2A}AR, α_{2A}-adrenergic receptor; NPY2R, neuropeptide Y type 2 receptor; AT1A, angiotensin II receptor; A_{2A}AR, A_{2A} adenosine receptor; n.50 residues, most conserved residues in TMHn (*11*); PDB, Protein Data Bank; TMH, transmembrane helices; WT, wild type; 5-HT_{2A}R, serotonin 2A receptor; MC-SCV, Monte Carlo-scaled collective variable; OCC, open−close cycle; 310-OCC, open−close cycle at 310 K; HCs, high-temperature ("hot") conformations; OHC-1210, open−heat−close cycle at 1210 K; LC_αrmsd, local C_α atom root-mean-square deviation; β_1IL2dm, β_1AR double mutant; β_2IL2dm, β_2AR double mutant.

Published on Web 11/09/2010

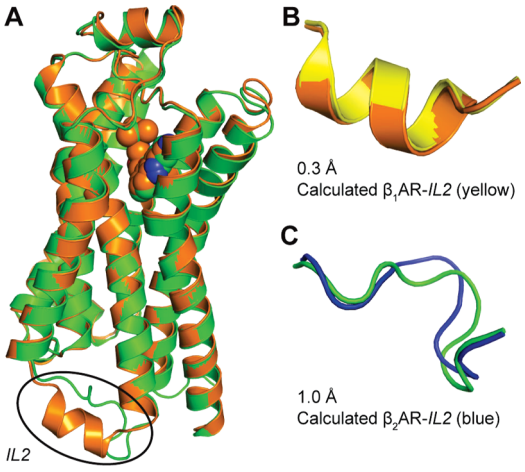

FIGURE 1: Structures of *IL2* in β_1AR and β_2AR. (A) Superposition of the TMH domains of the crystal structures of β_1AR (orange) (*44*) and β_2AR (green) (*45*) using their seven n.50 residues (*24*, *55*) yields a backbone rmsd of 0.6 Å for the TMH. Note the large difference in the structures of *IL2* (indicated in the oval). (B) *IL2* in β_1AR calculated with MC-SCV (yellow) is an α-helix, with a backbone rmsd of 0.3 Å to the α-helix in the crystal structure (orange). (C) *IL2* in β_2AR calculated with MC-SCV (blue) is an L-shaped strand with a backbone rmsd of 1.0 Å to the crystal structure (green).

in solution but adopts a helical conformation in the presence of 2,2,2-trifluoroethanol or negatively charged model membranes (*20*). An NMR study suggested that the major conformation for *IL2* in α_{2A}AR is α-helical (*21*). Crystallography has captured an L-shaped nonhelical conformation of this loop in rhodopsin (*22*) and β_2AR, but a helical one in β_1AR and A_{2A} adenosine receptor (A_{2A}AR) (*23*). Notably, these three receptors (β_1AR, β_2AR, and A_{2A}AR) are very similar in overall molecular structure. In particular β_1AR and β_2AR, with 67% sequence identity, have a backbone "global" rmsd of 0.62 Å [based on superposition of the backbones of the seven n.50 residues, the most conserved residues in seven transmembrane helices (TMH) as defined in ref *11*]. Given the high sequence homology of β_1AR and β_2AR (70% in TMH regions), and the fact that their *IL2* loops differ by only two chemically similar residues (Arg vs Lys and Met vs Leu in β_1AR and β_2AR, respectively), the remarkable difference observed crystallographically in the *IL2* conformation was unexpected (Figure 1A). The hypothesis underlying the present study was that the observed differences reflect different propensities for adopting either form of loop conformation, but that both can be achieved by the compared GPCRs, albeit with different probabilities.

The importance of a transition between the two conformational families of the *IL2* is substantiated by ample experimental data, briefly outlined above, which suggest that the functional state (i.e., active or inactive) of *IL2* in β_1AR and β_2AR is controlled by its secondary structure and that this control may be general for *IL2* in other class A GPCRs. Thus the central question is one of commonality, not difference, i.e., (i) is it reasonable to conclude that the helical form of the loop is associated with the active form, and (ii) is there an explanation for the difference captured by the crystal structures that accommodates this conclusion? Within the constraints defined by the experimental findings, we have used a modified Monte Carlo (MC) simulation approach (see Methods) to identify the determinants for the structural variability of wild type (WT) and mutant forms of *IL2*, and how these determinants modulate the observed functional properties of *IL2* in β_1AR and β_2AR. The modified MC simulation approach used here (see Methods) determines an approximation of the absolute minimum free energy ensemble, which is necessary to carry out the function-related analysis reported in this work. This capability allows us to identify not a single, frozen conformation, but (i) the ensemble of conformations that can be adopted by the various loops, (ii) the possibility that all of the GPCRs have some probability for adopting the helical form of IL2, and (iii) the structural determinants for differences in the propensity for selecting a structure in the WT, unliganded form, which might also explain the different conformations observed in the crystal structures.

The experimental findings observed in the adrenergic receptors were recapitulated in other cognate GPCRs, including the serotonin receptor, $5HT_{2C}$R (*14*). Although crystal structures are not yet available for the serotonin receptors, all loops of the serotonin 2A receptor ($5HT_{2A}$R) were calculated (*24*) for an earlier homology model based only on rhodopsin (*25*). For the present studies a refined homology model was built on the basis of rhodopsin and β_2AR crystal structures, and the loops were rebuilt using this updated model in order to examine the determinants for the structural variability and its functional consequences. With the modeling and simulation approaches, we answer here a set of questions that are essential for understanding the functional role of structural flexibility in the *IL2* region, and the relation to the molecular details revealed by the structural determinations: (i) are the two conformations found for *IL2* in β_1AR and β_2AR accessible to both receptors, and if so, (ii) what is the determinant for the helical structure of *IL2* in β_1AR while in β_2AR it is an L-shaped strand (e.g., the protein context, or the differences in the sequence of *IL2*)? (iii) Do the structural properties of *IL2* determined for β_1AR and β_2AR extend to those calculated for the refined model of $5HT_{2A}$R, and (iv) how does the mutation of the functionally important proline at position 3.57 (*14*) affect the secondary structure preferences of *IL2*?

METHODS

Loop Modeling with Monte Carlo-Scaled Collective Variables. The loop modeling algorithm is based on searching conformation space for the absolute free energy minimum ensemble, i.e., the cluster of conformations that belong to the absolute free energy minimum of the system. The computational algorithm consists of Monte Carlo (MC)-simulated annealing followed by a MC-scaled collective variables (*26*) approach (here the complete algorithm is termed the MC-SCV). It has been described in detail in previous publications (*24*, *27*, *28*), and its application has been illustrated in several systems (*24*, *27*, *29*, *30*). The approach was programmed into CHARMM (*31*) in the context of the PAR22 (*32*) force field. The basic strategy of the method consists of tethering the loop (or larger variable segment) to its attachment point at either the N- or C-terminus. At the other terminus a dummy residue is attached that is identical to a fixed target residue with known coordinates (this dummy residue makes no contribution to the system's potential energy, but only enters the total energy via a harmonic force term). Using an increasing harmonic force [effected by increasing the force constant (k) using a schedule $k_{i+1} = 10k_i$], the dummy residue at the open end of the loop is driven toward the target residue [the process can be reversed, i.e., the loop reopened, by decreasing k ($k_{i+1} = k_i/100$), although the final open conformation will not necessarily be the same as in the previous open state]. One such

complete opening and closing of the loop is designated as an "open−close cycle" (OCC) or *T*-OCC, where *T* refers to the temperature at which the OCC is carried out. As described in the Supporting Information, step 3 consists of open−close cycles where the loop is opened, heated to a high temperature, e.g., 1210 K, and closed at the high temperature; a complete cycle of this type is termed OHC-*T*. In the MC-SCV the solvent is modeled as a continuum using the screened Coulomb potential-implicit solvent model (SCP-ISM) in which the macromolecular system is assumed to be immersed in a fluid characterized by a sigmoidal screening function. The method has been described in detail (*33*) and shown to yield reliable results in various applications such as molecular dynamics simulations (*34*, *35*), and calculation of pH-dependent electrostatic effects in proteins (*36*−*39*). The SCP-ISM was programmed into CHARMM (*31*) and has been generally available in the distribution package for several years.

The analysis reported below requires representations of the native ensembles of WT and various mutations of *IL2* from several GPCRs. By comparing the calculated populations of secondary structures adopted by *IL2* in the ensembles, we estimate the relative stability of various classes of conformations. This analysis is similar to an earlier study in which it was shown that only the naturally occurring mutations in the autosomal disease Noonan syndrome (*40*) caused a shift in the active state−inactive state equilibrium, which results in a "gain of function" (*29*). This finding from the calculations was later verified experimentally (*41*). Additional details of the methodology and loop closing protocol are given in the Supporting Information.

The ensembles resulting from the 310-OCCs carried out in step 4 of the protocol (see the Supporting Information) are used to identify a good representative of the native ensemble. Because the native funnel is thought to be a rather narrow minimum surrounded by high peaks, a 310-OCC started from a conformation that is a member of the native ensemble will generate a condensed ensemble with small rmsd and energy fluctuations, whereas a 310-OCC started from a contribution far from the native funnel will generate a diffuse ensemble with a large rmsd and energy range. That this indeed is the case can be seen from Figure 5 of ref *28*, although it is noted that there also is another condensed ensemble with higher energy than the native ensemble.

To differentiate between the absolute free energy minimum ensemble and nearby secondary minima, a ranking is defined on the basis of a Helmholtz-like free energy defined by $\Delta\Delta A = \Delta A - E_0$, where $\Delta A = E_{\min} - RT\ln Q$, and $Q = \sum_{i=1}^{M} exp[-(E_i - E_{\min})/(RT)]$, with M being the number of replicas used in the Monte Carlo calculation and $E_{\min}$, E_0, and E_i representing the minimum energy of the given ensemble, the reference energy, and the energy of the ith conformation in the distribution, respectively. The ensemble with the lowest ΔA (or $\Delta\Delta A$) is assumed to be the best representative of the native ensemble. The minimum ΔA can be determined by iterating steps 3 and 4 until convergence is achieved. For most constructs, five low-energy structures from step 3 were selected for step 4 except for the P3.57A mutant in β_1AR, for which seven step 3 low-energy structures were selected.

Helicity Analysis of the IL2 Structure. The STRIDE algorithm (*42*) in VMD (*43*) was used to determine helicity for residues at positions 3.57−3.63 in *IL2* that correspond to the seven positions that assume a helical conformation in β_1AR (*44*) and A_{2A}AR (*23*). If all seven residues are designated as α-helix by STRIDE, the conformation is labeled "helix". If fewer than seven residues are designated as α-helix, the conformation is labeled "partial helix". "Helixlike" structures are defined as those with a local C_α atom rmsd (LC_αrmsd, based on the superposition of the segment only) of no greater than 2 Å compared to the crystal structure of *IL2* in β_1AR (*44*), but not defined as helix or partial helix according to STRIDE. Similarly, "β_2AR-like" structures are defined as those with an LC_αrmsd no greater than 2.5 Å compared to the crystal structure of *IL2* in β_2AR (*45*) (note that a less stringent local rmsd cutoff is used to define structures similar to *IL2* in β_2AR, which is an L-shaped strand). Finally, using the STRIDE nomenclature, the secondary structure distribution of an ensemble is annotated as helix/partial helix/helixlike/β_2AR-like/random coil.

Homology Modeling. A homology model of the TMH portions of 5-HT_{2A}R was built with MODELER 9v1 (*46*) using as templates the crystal structures of β_2AR [PDB entry 2RH1 (*45*)] and bovine rhodopsin [PDB entry 1U19 (*47*)]. The resulting 100 models were closer to β_2AR than to rhodopsin, especially in the TMH regions. The slight difference between the new models of 5-HT_{2A}R and β_2AR lies mostly in TMH1. In more than 90 conformations, the orientation of TMH1 is similar to that of β_2AR, while in the remaining structures, the orientation of TMH1 was between those of TMH1 in β_2AR and rhodopsin. After these 100 models had been clustered with nmrclust (*48*), a representative structure was selected from the most populated cluster as the new 5-HT_{2A}R model. The new model was closer to β_2AR with a small all-TMH backbone rmsd of 0.6 Å to β_2AR (2.1 Å to rhodopsin); the individual TMH rmsd to β_2AR was < 1 Å except for TMH7, for which it was 1.2 Å, while the individual TMH rmsds to rhodopsin were 1.5−3.2 Å.

Side chain rotamers were added with SCWRL3.0 (*49*), and the results were compared with the MODELER-predicted rotamers. If rotamers predicted by these two programs were similar (defined as all-atom rmsd of < 1.5 Å), we kept the MODELER-predicted structures. If rotamers were predicted differently by the two methods, visual inspection was performed to choose those that could form specific interaction networks, i.e., conserved structural motifs and functional microdomains including the DRY motif (*25*, *50*). After minimization, loop coordinates were calculated for this model with MC-SCV as detailed above.

RESULTS AND DISCUSSION

Structural Properties of IL2 in β_1AR and β_2AR. (*i*) *Validation of MC-SCV in Calculations of IL2 with Known Structures*. To validate the method for the specific analysis presented here, we modeled *IL2* in β_1AR and β_2AR with the protocols detailed in Methods. A preliminary report was given elsewhere (*51*). The 310-OCC protocol was applied to *IL2* conformations in these structures to generate ensembles, each consisting of 128 conformations of *IL2*. Five lowest-energy conformations were selected from those; a new set of 128 replicas was generated for each (i.e., a total of 640 replicas), and each replica was subjected to the OHC-1210 runs defined above. When the *IL2* was fully open at 1210 K, the helix in β_1AR melted while it was allowed to sample conformational space freely. However, upon closing even at this temperature, nearly 200 melted conformations of a total of 640 structures refolded into helices, and these conformations had lower energies than the nonhelical conformations. The lowest-energy conformation had a backbone rmsd of 0.3 Å against the crystal structure (Figure 1B). In the parallel procedure for *IL2* in β_2AR at this high temperature, the

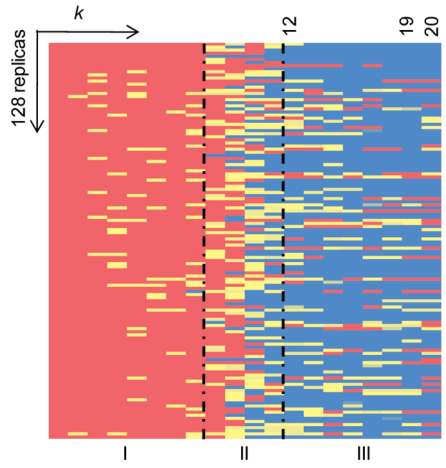

FIGURE 2: Conformational transitions of *IL2* in β_1AR during OHC-1210. The lowest-energy conformation from step 2 was replicated 128 times for OHC-1210, and the helicity of these 128 replicas was monitored during OHC-1210. Helicity is color-coded and shown as a function of the harmonic constant k and temperature, with red indicating that all seven residues in *IL2* (PFRYQSL) form a helix, yellow that some residues form a partial helix, and blue that none of the residues forms a helix. The plot is divided into three regions: I, opening at 310 K with k decreasing in steps of $k_{i+1} = k_i/100$; II, heating to 1210 K with constant k; and III, closing with increasing k ($k_{i+1} = 10k_i$).

Table 1: Distribution of Conformations in OHC-1210 Ensembles of the WT and P3.57A Mutant *IL2* in β_1AR

	ensemble[a]	helix[b]	partial helix[c]	helixlike[d]	β_2AR-like[e]	random coil[f]
WT	1	25	11	13	13	66
	2	22	7	19	10	70
	3	31	9	9	11	68
	4	18	14	9	8	79
	5	31	13	10	8	66
	total[g]	127	54	60	50	349
P3.57A	1	3	2	1	6	116
	2	3	0	1	6	118
	3	2	2	1	14	109
	4	1	4	0	4	119
	5	2	2	1	4	119
	total[g]	11	10	4	34	581

[a]Five lowest-energy conformations were selected from step 2 (310-OCC) of the WT and P3.57A mutant *IL2* in β_1AR, and each was replicated 128 times for OHC-1210 to generate five hot (OHC-1210) ensembles. Ensembles are ranked by the energies of their starting conformations from 310-OCC. [b]Number of complete helices. [c]Number of partial helices. [d]Number of helixlike structures. [e]Number of β_2AR-like conformations (see Methods for definitions). [f]Number of random coils in each hot ensemble. Random coils are conformations that are none of the above. [g]The total number of helices, partial helices, helixlike conformations, β_2AR-like conformations, and random coils in five hot ensembles of the WT and P3.57A mutant *IL2* in β_1AR.

loop folded back to conformations similar to the crystal structure with 247 conformations having a local backbone rmsd of < 1.0 Å [the lowest-energy conformation had a backbone rmsd of 1.0 Å against the crystal structure (Figure 1C)].

An important issue for validating the procedure is to ascertain that the final results, when the loops are closed, are independent of the starting conformations, i.e., all memory of the initial conformations has been lost. This validation is illustrated by the results shown in Figure 2 for the conformational changes of β_1AR-*IL2* during OHC-1210. The columns show the progression with changing the harmonic constant (the k parameter) and elevating the temperature for the 128 replicas that make up the rows of the matrix. In the leftmost columns, indicating the degree of helicity (highest in red, none in blue) during the opening phase at 310 K, all replicas are seen to have maintained their helical conformations. With progression to the right, some begin to lose helicity when heated, and in the rightmost columns more and more replicas are seen to have lost helicity during the closing phase at 1210 K (for example, from column 12 to 19 the number of helical conformations decreases steadily from around 54 to 26 in column 19). However, the most striking result in Figure 2 is that in the final column (20) the number of helical conformations has increased back to 36 (of 128), although only three replicas retained some helicity throughout the closing process, while the others melted completely (shown by the blue in the columns to the left of 20 in Figure 2). Transition of a conformer from red to blue (in Figure 2) is taken to signify that all memory of the starting helix has been lost. Thus, the validation tests confirm that MC-SCV at 1210 K can efficiently sample conformational space during OHC-1210, and that the procedure reproduces the structures for *IL2* in β_1AR and β_2AR independently of the starting conformation. This conclusion is further supported by earlier calculation of loops in rhodopsin (*28*) using the MC-SCV protocol in which OHC-T at temperatures ≥ 1310 K were found to conserve only one or two of 128 replicas that were similar to the original starting conformation with an rmsd < 1 Å, while the mean rmsd went up to 5.9 Å and maximum values of up to 16 Å for 1810 K (see Table 3 of ref *28*).

The starting structures for the above analysis were the *IL2* crystal structures of the two adrenergic receptors. Since the loops are usually located at the surface of the protein it is possible that lattice contacts with neighboring molecules would affect their structure in a manner not accounted for in the calculations (see Methods). Indeed, it had been proposed that helical *IL2* would not be possible in β_2AR structures because it would clash with its crystal lattice contacts, and thus helical *IL2* was likely the physiologically relevant structure in all βAR structures (*44*). To explore this issue the MC-SCV protocol [for loop structure prediction (*28*)] was used to predict the structure of the *IL2* loop in β_2AR starting from a completely extended (i.e., arbitrary) structure, and the calculations yielded an rmsd range of 1−1.5 Å from the superposition of the loop structures in the ensemble on the crystal structure. This rmsd range indicates that the structures of all members of the ensemble are essentially identical to the crystal structure, so that any additional interactions between *IL2* and the crystal environment have an only a minimal effect on the observed structure, thus validating the calculations on WT and mutant constructs of *IL2*.

(*ii*) *Accessible Conformations for IL2*. The validated procedure was used to address the basis for the puzzling difference in the crystallographically observed structures of *IL2* in β_1AR and β_2AR in spite of the similarity in the loop sequence and overall molecular structure of these two GPCRs. Two key questions were addressed in this respect: first, are both classes of loop conformations accessible to each protein, and second, which components of the molecular environment determine the preferred conformation and might control the interconversion?

To explore these issues, high-temperature conformations (HCs) obtained from OHC-1210 and OHC-1435 were compared to the crystal structure conformations of *IL2* in β_1AR and β_2AR to assess if OHC ensembles had sampled both helical and nonhelical conformations in both receptors. For β_1AR we found

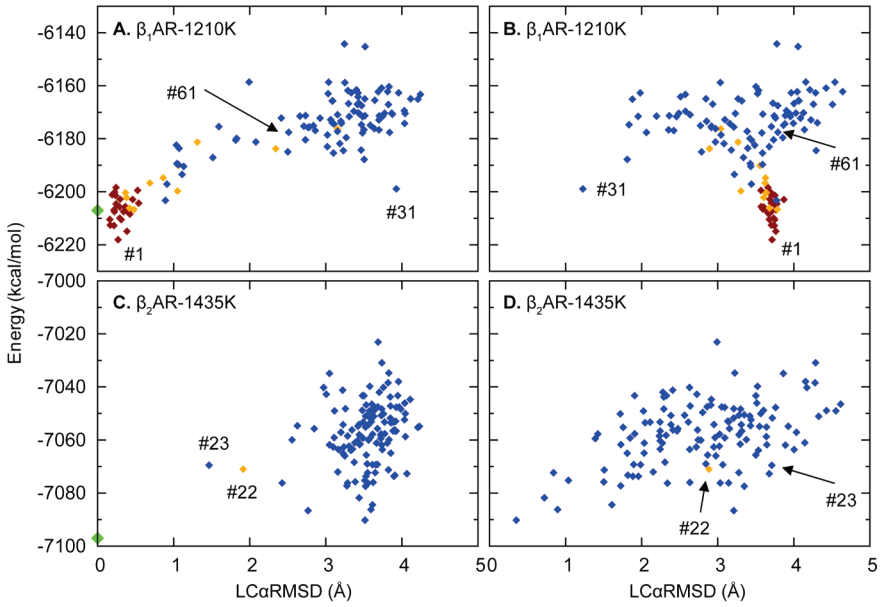

FIGURE 3: Plots of energy vs LC_αrmsd for hot ensembles of *IL2* in β_1AR and β_2AR. (A and B) The OHC-1210 ensemble of *IL2* in β_1AR obtained from the lowest-energy conformation in step 2 with LC_αrmsd calculated relative to the X-ray structure of β_1AR (A) and β_2AR (B). (C and D) Hot ensemble of *IL2* in β_2AR obtained from OHC-1435 with LC_αrmsd calculated as described above. Each symbol represents an individual HC in the ensemble, OHC-1210 (β_1AR) or OHC-1435 (β_2AR). Conformations are colored by helicity assigned by STRIDE (*42*) (see Methods): dark red, a complete helix; orange, a partial helix; blue, a nonhelical structure; and green, the X-ray structures of *IL2* in β_1AR (A) and β_2AR (C). Individual replicas discussed in the the text are labeled by their energy ranking (indicated by the number sign) in their own ensembles.

that of the 640 HCs obtained from OHC-1210, a total of 38% are helical, and notably, there are also 50 (8%) conformations similar to *IL2* in β_2AR (see Table 1, WT). For example, in ensemble *1*, 13 (10%) of 128 replicas are β_2AR-like with an LC_αrmsd of ≤2.5 Å (Figure 3B), such as conformer #31 (where #*x* designates the energy ranking of the conformer in its ensemble, indicated in Figure 3A,B, illustrated in Figure 4a), but their energies are higher than those of helical conformations (Figure 3A,B). This distribution of the conformers is typical for the five lowest-energy ensembles of β_1AR given in Table 1. Note that the same conformational types are also sampled at 1435 and 1660 K.

IL2 in β_2AR also sampled both helical and nonhelical conformations during OHC at high temperatures (Figure 3C,D). Interestingly, OHC-1210 did not produce any helical structures, but heating the loops further, to 1435 K, did. OHC-1435 sampled a partial helical structure #22 labeled in Figure 3C, and a helixlike structure #23 with an LC_αrmsd of 1.47 Å (shown in Figure 3C) when superimposed on β_1AR-*IL2*. However, most low-energy structures are similar to *IL2* in β_2AR (Figure 3C,D). Further heating did not change the distribution, as OHC-1660 gave similar results.

Together, the results obtained separately for *IL2* in the two receptors indicate that the helical and nonhelical conformations of *IL2* can be interchanged in the high-temperature simulations that increase accessibility to rare events. These findings suggest that although the different GPCRs have clear preferences for one conformation of *IL2* or the other, both conformations are available to the loop and are visited with different probabilities.

(*iii*) *Structural Preference of β_1AR-IL2*. To quantify the structural preference of *IL2* in β_1AR, 18 structures obtained from OHC at different temperatures were selected with the following attributes: nine were helical (including helix, partial helix, and helixlike conformations), five were β_2AR-like, and four were random structures (neither helical nor β_2AR-like) (see Table S1 of the Supporting Information for detailed results from the simulations). One hundred twenty-eight replicas were created from each of these structures for use in 310-OCC. Analysis of the resulting ensembles showed that low-energy helical conformations remain helices and helical ensembles have lower energies compared to other ensembles (Figure 4b and Table S1). In addition, one partial helix (#4) and one helixlike conformation (#3) from OHC-1660 (Figure 4c,d and Table S1) yielded complete helices in their 310-OCC ensembles with an LC_αrmsd against β_1AR of ≪1 Å (see Figure 4). Interestingly, both random and β_2AR-like structures obtained from OHC (Figure 4e,f) also turned into complete helices with energies improved after the second run of 310-OCC and converged after the third 310-OCC (Table S1). The calculations thus established a clear trend to transit from nonhelical conformations to helices at 310 K, with uniformly lower energies for the helical solutions compared to nonhelical structures. This finding is in good agreement with the crystallographic data suggesting that the helical conformation represents the native conformation of *IL2* in the β_1AR.

(*iv*) *Structural Preference of β_2AR-IL2*. Comparison of results in panels A and B of Figure 3 to those in panels C and D of Figure 3 shows that the tendency of *IL2* in β_2AR to form helical conformations at high temperatures is considerably smaller than for β_1AR, and occurs only at temperatures of >1210 K. For example, only one of 128 structures obtained from OHC-1435 in β_2AR is a partial helix, one is helixlike, while 48 (including the low-energy ones) are β_2AR-like structures. The remaining 70 structures are random coils. To explore these conformations further, we selected 11 structures (see Table S2 of the Supporting Information) [seven β_2AR-like (five lowest-energy conformations from OHC-1210, #1 from OHC-1435 and #2 from OHC-1660), two partial helical or helixlike HCs (#22 and #23 from OHC-1435), and two random structures (#1 and #13 from OHC-1660) (Table S2)] and created 128 replicas of each for 310-OCC. After 310-OCC, the β_2AR-like conformations in all the ensembles were found to have lower $\Delta\Delta A$ values than partial helical or helixlike conformations obtained from #22, #23, and #13. In contrast to the behavior of *IL2* in β_1AR, none of the

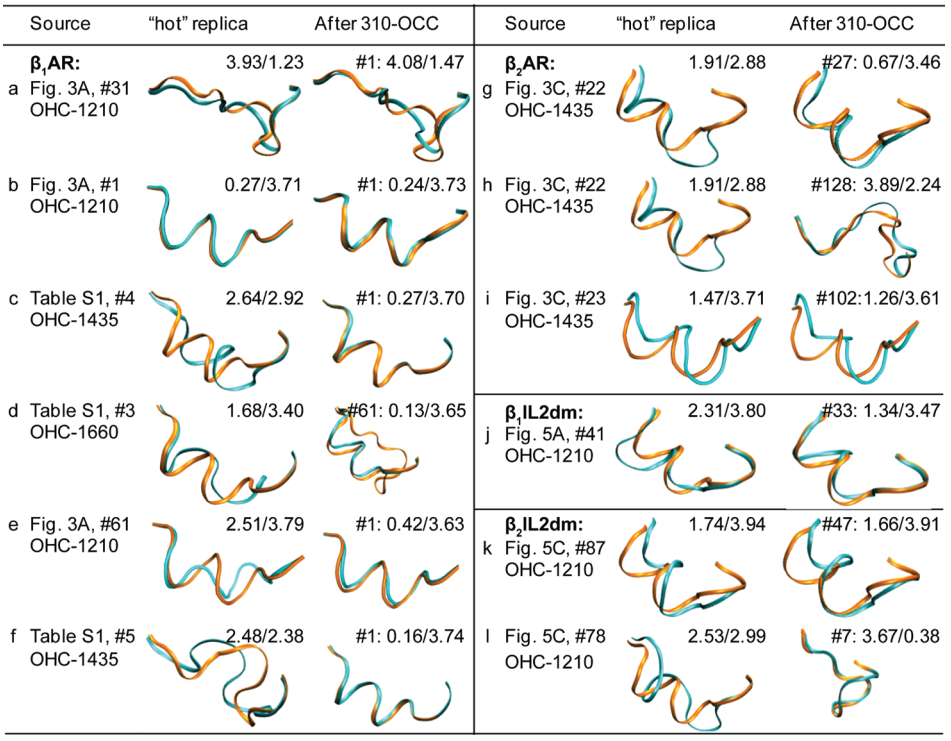

FIGURE 4: Conformational transitions during 310-OCC following OHC. Conformations of sample replicas obtained from OHC at high temperatures and their conformations after 310-OCC. The Source column identifies the structural context of the loop, the figure or table that discusses this loop in the paper, the energy ranking of the HC in its ensemble (indicated by the number sign), and the OHC temperature. The calculated loops (cyan) and those from the X-ray structures (orange; the helical one is from β_1AR and the nonhelical one from β_2AR) are shown in their orientation when the receptors are globally superimposed. The numbers in the inset in the hot replica and the After 310-OCC columns are LC_αrmsds of the cyan replica relative to β_1AR/β_2AR. For the 310-OCC replica, the energy ranking in its ensemble is also denoted in front of its LC_αrmsds to β_1AR/β_2AR.

partial or helixlike conformations folded into complete helices (Figure 4g–i). The number of partial helices (Figure 4g, #27, and Figure 4i, #102) in the resulting 310-OOC ensembles is much smaller than for the β_1AR calculation (only two for β_2AR as compared to 20–100 for β_1AR), but like the latter, transitions to the alternative conformation are observed with 310-OCC (Table S2). Thus, the simulations indicate that *IL2* in β_2AR overwhelmingly prefers the nonhelical conformation represented in the crystallographic findings (*45*). Several considerations support this conclusion: (i) after 310-OCC the nonhelical β_2AR-like conformers always have lower energies; (ii) hot helical conformations did not fold further into complete helices and did not generate ensembles with large numbers of helical conformations during 310-OCC (contrary to what was observed with *IL2* in β_1AR); (iii) any transition from β_2AR-like conformations to helical ones took place at temperatures higher than 1210 K, where the helical conformations in β_1AR had converted to β_2AR-like conformations.

(*v*) *Determinants of IL2 Structure*. As shown in the previous sections, both the helical and β_2AR strand conformations are accessible to *IL2* in β_1AR and β_2AR. Nevertheless, it is also clear that β_1AR selects the α-helical conformation because it is of lowest free energy in this protein, whereas in the β_2AR the strand is of lowest free energy. These results from the simulations on the WT receptors are in complete agreement with the crystallographic findings and now allow the source of the structural regulation to be explored. First, the role of the *IL2* sequence and the structural context of its protein environment were considered to identify the determinant factors for the structural preference of *IL2* in the two similar receptors. To address the sequence determinant, reciprocal double mutant constructs of *IL2* were inserted into the two receptors, interchanging the corresponding residues at positions 3.59 and 3.64 (i.e., Arg/Lys and Met/Leu for β_1AR/β_2AR). The 128 replicas of the β_1AR double mutant (β_1IL2dm) and the β_2AR double mutant (β_2IL2dm) were relaxed with the 310-OCC protocol, and the resulting five lowest-energy conformations were selected for OHC-1210. The distribution of the resulting HCs shows that the mutants behave like the WT (compare Figures 3 and 5 panel by panel, and see Table S3 of the Supporting Information). For β_1IL2dm, the secondary structure distribution is (106/53/54/55/372) to be compared with the β_1AR distribution of (127/54/60/50/349). Table S3 further shows that the distributions of the individual ensembles in each panel are similar and that distributions in panels A and B are similar as well. An alternative approach to constructing the double mutants is to use chimeras, e.g., by inserting *IL2* from β_1AR into β_2AR and then applying the same protocol as for the double mutants. The results from the double mutant calculations suggest that the propensity for forming β_2AR-like conformations should increase in the chimera, which is indeed the case, as their number increases from 50 (of 640) conformations in the WT to 56 in the chimera. The other chimera (*IL2* from β_2AR into β_1AR) behaves similarly, but now the propensity to form helical structure should increase, which it does from zero helixlike conformations in the WT to three in the chimera. We note that given the structural preferences of *IL2* in β_1- and β_2AR (helix in the former and the L-strand in the latter) the chimeras are much farther from convergence than the double mutants, so that most calculations were carried out using the double mutant constructs.

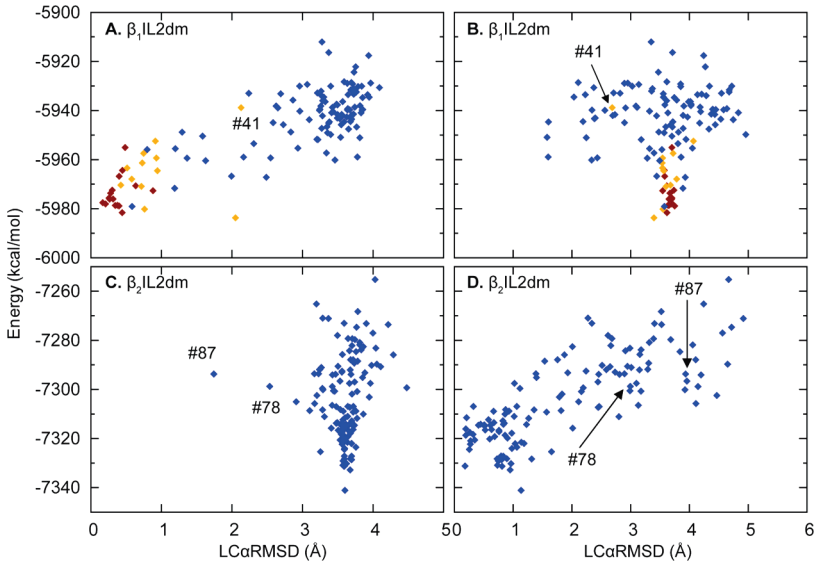

FIGURE 5: Plots of energy vs LC_αrmsd for hot ensembles of the mutant constructs β_1IL2dm and β_2IL2dm. (A and B) OHC-1210 ensemble of β_1IL2dm obtained from the lowest-energy conformation in step 2, plotted as in Figure 3 except that here it is the mutant that is compared to the X-ray conformation of *IL2* in β_1AR and β_2AR. For details see Figure 3. (C and D) OHC-1210 ensemble of β_2IL2dm obtained from the second lowest-energy conformation in step 2, plotted as in panels A and B.

Figures 3A,B and 5A,B show the distributions of the OHC-1210 ensembles (starting from the conformation with the lowest energy in its 310-OCC ensemble) of β_1AR and of β_1IL2dm, respectively. Similar to WT (Table S1), most low-energy conformations in this β_1IL2dm ensemble are helixlike (Table S4 of the Supporting Information). After 310-OCC, the five lowest-energy conformations from the OHC-1210 ensembles form mostly helical structures (Table S4). Helical ensembles have lower energies than those obtained from hot β_2AR-like conformations (Table S4). Similar to WT, a nonhelical conformation #41 from OHC-1210 also converts to a helix during 310-OCC (Figure 4j). The β_2IL2dm also exhibited behavior similar to that of its corresponding WT (see Table S3, panels C and D). Interestingly, the second ranking OHC-1210 ensemble of β_2IL2dm sampled a helixlike conformation [#87 (Figure 5C,D)], although the WT did not at this temperature. Like WT, after 310-OCC, ensembles from hot β_2AR-like conformations have energies lower than those of other ensembles (Table S5 of the Supporting Information). The helixlike conformation [#87 (Figure 4k and labeled in Figure 5C,D)] and the one with the second smallest LC_αrmsd [#78 (Figure 4l)] to β_1AR-*IL2* from OHC-1210 did not turn into complete helices and did not produce a large number of partial helices (Table S5).

The similarity that both double mutants show in their conformational preferences to their corresponding WT structures in all the conformational searches supports that the differences in the sequence of these *IL2* loops cannot be the main determinant for their differing structural preferences in the cognate GPCRs, i.e., helical for β_1AR and nonhelical for β_2AR. In contrast, comparison of panels A and B with panels C and D in Figures 3 and 5, respectively, shows very different energy landscapes in the β_1AR panels than in the β_2AR panels. This finding, together with the elimination of the loop's sequence as the main determinant of conformation, indicates that it is the action of the protein−solvent environment on the loops that determines their preferred secondary structure. Thus, the biology of the receptors is not different, but the loop undergoes transitions between the helical and nonhelical conformations as a function of the state of the receptor. Since the two crystal structures were obtained from different conditions they appear to represent different states.

Structural Properties of IL2 in 5-HT$_{2A}$R. In the earlier calculation of the *IL2* structure in the 5HT$_{2A}$R (*24*) a strand conformation similar to that in rhodopsin was assumed, as shown in Figure 6A, with a local backbone rmsd of 1.61 Å for the seven residues from position 3.57 to 3.63 in the sequence. In the β_2AR crystal structure (*45*) the local backbone rmsd is 1.47 Å. Starting from this loop, we recalculated the structure of *IL2* in the updated 5-HT$_{2A}$R model in the following way: First, the loop was attached to the intracellular end of TMH3 in the new homology model and closed using MC-SCVs. Then, 310-OCC was carried out for the 96 structures (see Methods) to fully relax them in the field of the updated 5-HT$_{2A}$R structure. From the resulting conformations, the four lowest-energy structures were selected, each replicated 96 times for OHC-1210. The four resulting ensembles are listed in Table S6A of the Supporting Information. As for the adrenergic receptors, both helical and β_2-like conformations are seen to be accessible to the predicted *IL2* in 5HT$_{2A}$R; from the resulting ensembles, the five lowest-energy conformers (of which the lowest-energy conformer and two others came from ensemble *3* in Table S6A) were selected, each replicated 128 times for 310-OCC. Notably, even at a temperature as high as 1210 K, some loops transitioned to helical conformations when the loop was closed (Table S6A, ensemble *3*), and these were conserved during the subsequent 310-OCC. The result is an ensemble highly populated with helices [123 complete helices and four partial helices out of 128 replicas (see Table S7, WT)]. This ensemble has lower energies compared to other ensembles and was taken as the native ensemble. These results strongly support our contention that the conformation of *IL2* is controlled by the protein−solvent environment because here the *IL2* sequence is identical in both calculations.

Although the *IL2* sequence in 5-HT$_{2A}$R shares only one residue with those in β_1AR and β_2AR, i.e., P3.57, and it was modeled starting from a structure similar to β_2AR, the lowest-energy loop conformation in the resulting ensemble is similar to that of β_1AR-*IL2* [with a small local backbone rmsd of 0.48 Å (Figure 6B)]. Remarkably, *IL2* in 5-HT$_{2A}$R not only adopts a

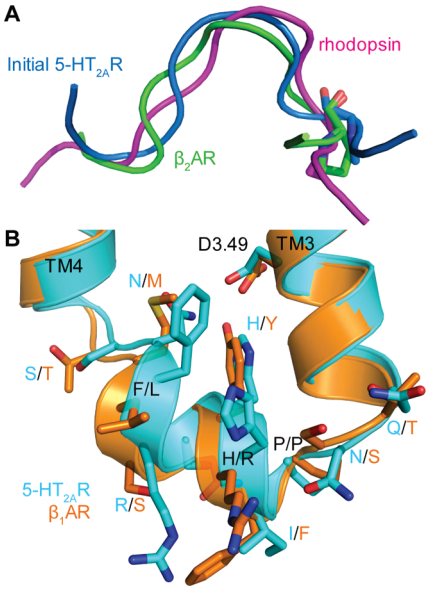

FIGURE 6: Conformations of *IL2* before and after MC-SCV remodeling in the new model of the 5-HT_{2A}R. (A) Previously calculated *IL2* (blue) in the old model has a local backbone rmsd of 1.61 Å against that in rhodopsin (magenta) and 1.47 Å against that in β_2AR (green) for seven residues (from position 3.57 to 3.63). *IL2* in rhodopsin and β_2AR were superimposed with that in 5-HT_{2A}R using backbones of residues from position 3.57 to 3.63. Residue Pro3.57 is shown in stick representation. (B) Superposition of the remodeled *IL2* (cyan) in the new model of 5-HT_{2A}R and *IL2* in the crystal structure of β_1AR (orange) (*44*). Partial TMH3, *IL2*, and partial TMH4 helices in 5-HT_{2A}R and β_1AR are shown as ribbons. Their *IL2* side chains are shown as sticks and labeled in the format of X/Y, with X denoting the name for residues in 5-HT_{2A}R and Y denoting the name for residues in β_1AR. In addition the side chain of the conserved D3.49 in the DRY motif is also shown in stick representation.

similar helical conformation but also maintains a similar fold (orientation to the rest of the receptor) to that in β_1AR (see Figure 6B). Moreover, side chains in 5-HT_{2A}R are predicted to have similar orientations to those in β_1AR, especially for residues 3.55Q/T (Q in 5-HT_{2A}R and T in β_1AR), 3.57P/P, 3.58I/F, 3.60H/Y, 3.61S/Q, 3.64N/M, and 3.65S/T. This helix-containing structure of *IL2* in 5-HT_{2A}R remained stable in a 350 ns MD trajectory obtained in an explicit environment of water and lipids (*52*).

Role of the Conserved Proline in the Preference for the Helix-Containing Conformation of IL2. As demonstrated experimentally (see the introductory section), *IL2* plays an important functional role in the activation of G-proteins and interaction with β-arrestin (*8*, *9*), and the P3.57A mutants have clearly different phenotypes. Moreover, the highly conserved proline at position 3.57 appears to be a key component in the regulation of *IL2* function. To understand this regulation, the effect of P3.57A on the structure of *IL2* was modeled starting from the β_1AR crystal structure and using the same protocol as for the WT. Like the WT, the original helices of the mutant *IL2* started to melt during OHC-1210, when the temperature was raised to 1210 K and the harmonic constraint was small (Figure 7A). However, in sharp contrast to the WT protein, very few conformers refolded into helices when the loop was closed (see Figure 7A). As shown in Table 1 the same phenomenon was observed in all five hot ensembles starting from different low-energy cold conformations. In total, only 25 of 640 mutant structures regained helical structures, compared to WT where 241 of 640 structures regained helical conformation (see Table 1).

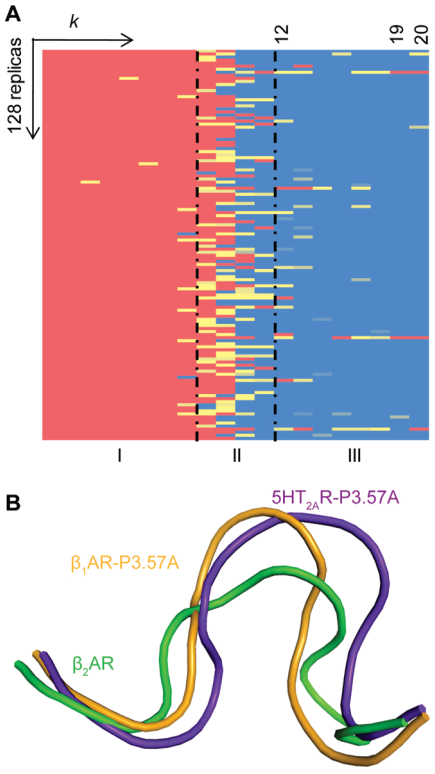

FIGURE 7: Conformational changes of the P3.57A mutant *IL2* in β_1AR. (A) Matrix of conformations annotated as in Figure 2. (B) Conformations of the P3.57A mutant *IL2* in 5-HT_{2A}R (purple) and β_1AR (orange) compared to WT *IL2* in β_2AR (green).

Overall, the destabilizing effect of the mutation results in many more mutant structures assuming a random coil conformation with LC_αrmsd up to 4.3 Å compared to the starting conformation even when the loops were fully closed. To search for the best representative of the native ensemble in the WT and mutant protein, the five lowest-energy HCs of the WT and the five lowest-energy HCs (including one β_2-like structure and four helices) of the mutant were selected for generating 310-OCC ensembles. Unlike the WT, the nonhelical HC did not yield helices after 310-OCC but only yielded β_2AR-like conformations (Figure 7B). For the mutant, the nonhelical ensemble has a lower energy [~5 kcal/mol (Table 2)] than the helical ones and thus would be a better representative of the native ensemble of the mutant. Furthermore, the low-energy regions of HCs of the mutant had more β_2-like structures while the low-energy regions of HCs of the WT are mostly helical structures. 310-OCC starting from the seventh lowest-energy mutant HC also generated a β_2AR-like ensemble with lower energies than those helical ensembles (data not shown). Taken together, the results show that the P3.57A mutation destabilizes the helical conformation of *IL2* in β_1AR, resulting in a β_2AR-like structure with a local backbone rmsd of 2.30 Å relative to *IL2* in β_2AR (Figure 7B).

To determine whether this mutation also reduces the helical content of the predicted *IL2* structure in 5-HT_{2A}R, steps 2−4 were repeated on that P3.57A mutant as for the WT structure. The behavior of the mutant *IL2* loop in 5-HT_{2A}R was found to be similar to the P3.57A mutant of β_1AR in that (i) helices started to melt when the temperature was raised to 1210 K during OHC-1210 but fewer regained helical structures compared to the WT (see Table S6B of the Supporting Information), (ii) after 310-OCC nonhelical conformations had lower energies compared to helical ones (Table S7), and (iii) the lowest-energy mutant was

Table 2: Conformations of WT and P3.57A Mutant *IL2* in β_1AR after OHC-1210 and 310-OCC

	starting conformation[a]		conformation distribution and energy of 310-OCC ensembles				
	conformation	energy ranking	helix[b]	partial helix[c]	helixlike[d]	β_2-like[e]	ΔA (kcal/mol)[f]
WT	helix	3	**115**	12	1	0	**−6226.03**
	helix	2	123	5	0	0	−6225.18
	helix	5	118	10	0	0	−6225.01
	helix	1	128	0	0	0	−6222.98
	helix	4	126	1	1	0	−6222.21
P3.57A	β_2-like	5	0	0	0	**128**	**−6260.51**
	helix	2	127	1	0	0	−6255.26
	helix	4	126	2	0	0	−6255.24
	helix	3	128	0	0	0	−6254.42
	helix	1	128	0	0	0	−6251.80

[a]Five lowest-energy conformations were selected from five OHC-1210 ensembles (step 3) of the WT and P3.57A mutant *IL2* in β_1AR, and each was replicated 128 times for 310-OCC to generate five "cold" ensembles. The conformation for the hot replica is defined in Methods and is ranked by energies of their starting conformation from OHC-1210. [b]Number of complete helices. [c]Number of partial helices. [d]Number of helixlike conformations. [e]Number of β_2AR-like conformations (see Methods for definitions) in each 310-OCC ensemble. [f]The energy ΔA of the 310-OCC ensemble was calculated as described in Methods. Bold denotes the dominant conformation in the 310-OCC ensembles or the 310-OCC ensemble with the lowest energy (ΔA).

also β_2AR-like with a local backbone rmsd of 2.02 Å relative to the *IL2* in β_2AR (Figure 7B). Thus the P3.57A mutation has the same destabilizing effect on the helical structure of *IL2* in $5HT_{2A}R$ as it did on the β_1AR loop, which is consistent with the well-known helix capping effect of proline (*53*).

CONCLUDING REMARKS

The results of this analysis for all the cognate GPCRs, and the findings from recently described extensive simulations supporting the transition to helical conformation (*54*), indicate that both the nonhelical L-shaped strand and helix-containing conformations of the *IL2* in the rhodopsin-like GPCRs β_1AR, β_2AR, and (model) $5HT_{2A}R$ are intrinsic conformations of *IL2* that can interconvert.

The structure of *IL2* in 5-HT_{2A}R calculated in the context of a refined structural model based on rhodopsin and β_2AR yielded a helical conformation similar to that of β_1AR. In agreement with a recent report that *IL2* in β_2AR transits into and maintains a helix in a microsecond MD simulation (*54*), we found that starting from an MD equilibrated structure of 5-HT_{2A}R (a snapshot taken at 200 ns) and carrying out 310-OCC and OHC-1210, the propensity for *IL2* in 5-HT_{2A}R to form helix is significantly increased and similar to that for *IL2* in β_1AR (data not shown).

Our results also identified a sequence dependence of the structural preference of *IL2*, to the extent that the helical form is strongly destabilized upon mutation of the conserved P3.57. However, for the WT systems the findings suggest that the protein context of the loop is the primary determinant of the conformational preference observed for the *IL2*s in β_1AR and β_2AR that are so highly similar in sequence. Significantly, receptor activation can produce large conformational rearrangements in the environment of *IL2* and thereby change the propensity for adopting the helical conformation. This suggests a direct mechanistic implication of our findings, related to ligand-induced modulation of the probability for helical conformation of *IL2*: We propose that the structural transition of *IL2* is part of the conformational change of these GPCRs that is required in order to achieve the "ligand-activated conformation". Indeed, the behavior of the P3.57A mutant of *IL2* in β_1AR and 5-HT_{2A}R suggests that the structural transition to the helical form is associated with activation, because the P3.57A mutation that we found here to decrease significantly the propensity of the loop to form helix also causes an observed decrease in β-arrestin binding and induced internalization (*14*). This makes the helical conformation of *IL2* the relevant form for binding β-arrestin, consonant with its being part of the ligand-induced active conformation. Given the apparently general characteristic of the *IL2* structural transition in the cognate receptors we studied, it becomes tempting to suggest that the crystal structure of β_2AR (*45*) with an *IL2* lacking the helical element might be closer to the inactive conformation. This is consistent with β_2AR in the crystal binding an inverse agonist, carazolol, whereas β_1AR and A_{2A}AR are bound to antagonists, which show no preference for the active versus inactive forms of GPCRs.

ACKNOWLEDGMENT

Computational support was provided by the National Science Foundation Terascale Computing System at the Texas Advanced Computing Center (TG-MCB080118N). We also acknowledge access to the computer facilities at the Institute of Computational Biomedicine of Weill Medical College of Cornell University.

SUPPORTING INFORMATION AVAILABLE

Additional discussion of the MC-SCV four-step protocol used to calculate the model structures of the WT and mutant *IL2* sequences and additional tables summarizing the energy and conformations for β_1AR-*IL2* (Table S1) and β_2AR-*IL2* (Table S2) after OHC and 310-OCC, the conformation distribution of β_1AR-*IL2*, β_2AR-*IL2*, β_1IL2dm, and β_2IL2dm after OHC-1210 (Table S3), the energy and conformation for β_1IL2dm (Table S4) and β_2IL2dm (Table S5), the conformation distribution for the WT and mutant (P3.57A) *IL2* in 5-HT_{2A}R after OHC-1210 (Table S6), and their energies and conformations before and after 310-OCC (Table S7). This material is available free of charge via the Internet at http://pubs.acs.org.

REFERENCES

1. Kobilka, B. K., and Deupi, X. (2007) Conformational complexity of G-protein-coupled receptors. *Trends Pharmacol. Sci. 28*, 397–406.
2. Park, P. S., Lodowski, D. T., and Palczewski, K. (2008) Activation of G protein-coupled receptors: Beyond two-state models and tertiary conformational changes. *Annu. Rev. Pharmacol. Toxicol. 48*, 107–141.

3. Burstein, E. S., Spalding, T. A., and Brann, M. R. (1998) The second intracellular loop of the m5 muscarinic receptor is the switch which enables G-protein coupling. *J. Biol. Chem. 273*, 24322–24327.
4. Chao, T. H., Ember, J. A., Wang, M., Bayon, Y., Hugli, T. E., and Ye, R. D. (1999) Role of the second extracellular loop of human C_{3a} receptor in agonist binding and receptor function. *J. Biol. Chem. 274*, 9721–9728.
5. Shi, L., and Javitch, J. A. (2002) The binding site of aminergic G protein-coupled receptors: The transmembrane segments and second extracellular loop. *Annu. Rev. Pharmacol. Toxicol. 42*, 437–467.
6. Shi, L., and Javitch, J. A. (2004) The second extracellular loop of the dopamine D_2 receptor lines the binding-site crevice. *Proc. Natl. Acad. Sci. U.S.A. 101*, 440–445.
7. Klco, J. M., Wiegand, C. B., Narzinski, K., and Baranski, T. J. (2005) Essential role for the second extracellular loop in C5a receptor activation. *Nat. Struct. Mol. Biol. 12*, 320–326.
8. Wess, J. (1998) Molecular basis of receptor/G-protein-coupling selectivity. *Pharmacol. Ther. 80*, 231–264.
9. Gether, U. (2000) Uncovering molecular mechanisms involved in activation of G protein-coupled receptors. *Endocr. Rev. 21*, 90–113.
10. Wong, S. K. (2003) G protein selectivity is regulated by multiple intracellular regions of GPCRs. *Neurosignals 12*, 1–12.
11. Ballesteros, J. A., and Weinstein, H. (1995) Integrated Methods for Modeling G-Protein Coupled Receptors. *Methods Neurosci. 25*, 366–428.
12. Raman, D., Osawa, S., Gurevich, V. V., and Weiss, E. R. (2003) The interaction with the cytoplasmic loops of rhodopsin plays a crucial role in arrestin activation and binding. *J. Neurochem. 84*, 1040–1050.
13. Moro, O., Lameh, J., Hogger, P., and Sadee, W. (1993) Hydrophobic amino acid in the i2 loop plays a key role in receptor-G protein coupling. *J. Biol. Chem. 268*, 22273–22276.
14. Marion, S., Oakley, R. H., Kim, K. M., Caron, M. G., and Barak, L. S. (2006) A β-arrestin binding determinant common to the second intracellular loops of rhodopsin family G protein-coupled receptors. *J. Biol. Chem. 281*, 2932–2938.
15. Kristiansen, K. (2004) Molecular mechanisms of ligand binding, signaling, and regulation within the superfamily of G-protein-coupled receptors: Molecular modeling and mutagenesis approaches to receptor structure and function. *Pharmacol. Ther. 103*, 21–80.
16. Weinstein, H. (2005) Hallucinogen actions on 5-HT receptors reveal distinct mechanisms of activation and signaling by G protein-coupled receptors. *AAPS J. 7*, E871–E884.
17. Visiers, I., Hassan, S. A., and Weinstein, H. (2001) Differences in conformational properties of the second intracellular loop (IL2) in $5HT_{2C}$ receptors modified by RNA editing can account for G protein coupling efficiency. *Protein Eng. 14*, 409–414.
18. Berg, K. A., Cropper, J. D., Niswender, C. M., Sanders-Bush, E., Emeson, R. B., and Clarke, W. P. (2001) RNA-editing of the $5\text{-}HT_{2C}$ receptor alters agonist-receptor-effector coupling specificity. *Br. J. Pharmacol. 134*, 386–392.
19. Dracheva, S., Lyddon, R., Barley, K., Marcus, S. M., Hurd, Y. L., and Byne, W. M. (2009) Editing of serotonin 2C receptor mRNA in the prefrontal cortex characterizes high-novelty locomotor response behavioral trait. *Neuropsychopharmacology 34*, 2237–2251.
20. Shida, C. S., Casallanovo, F., Regina, K., Nakaie, C. R., Paiva, A. C. M., Pertinhez, T. A., Gatti, R., Spisni, A., and Schreier, S. (2001) Conformation and dynamics of a GPCR intracellular loop (IL) in soluction and in the presence of model membranes, Biophys. J. (Annual Meeting Abstracts).
21. Chung, D. A., Zuiderweg, E. R., Fowler, C. B., Soyer, O. S., Mosberg, H. I., and Neubig, R. R. (2002) NMR structure of the second intracellular loop of the a2A adrenergic receptor: Evidence for a novel cytoplasmic helix. *Biochemistry 41*, 3596–3604.
22. Palczewski, K., Kumasaka, T., Hori, T., Behnke, C. A., Motoshima, H., Fox, B. A., Le Trong, I., Teller, D. C., Okada, T., Stenkamp, R. E., Yamamoto, M., and Miyano, M. (2000) Crystal structure of rhodopsin: A G protein-coupled receptor. *Science 289*, 739–745.
23. Jaakola, V. P., Griffith, M. T., Hanson, M. A., Cherezov, V., Chien, E. Y., Lane, J. R., Ijzerman, A. P., and Stevens, R. C. (2008) The 2.6 Å crystal structure of a human A_{2A} adenosine receptor bound to an antagonist. *Science 322*, 1211–1217.
24. Mehler, E. L., Periole, X., Hassan, S. A., and Weinstein, H. (2002) Key issues in the computational simulation of GPCR function: Representation of loop domains. *J. Comput.-Aided Mol. Des. 16*, 841–853.
25. Visiers, I., Ballesteros, J. A., and Weinstein, H. (2002) Three-dimensional representations of G protein-coupled receptor structures and mechanisms. *Methods Enzymol. 343*, 329–371.
26. Noguti, T., and Go, N. (1985) Efficient Monte Carlo method for simulation of fluctuating conformations of native proteins. *Biopolymers 24*, 527–546.
27. Hassan, S. A., Mehler, E. L., and Weinstein, H. (2002) in Lecture Notes in Computational Science and Engineering (Schlick, T., and Gan, H. H., Eds.) pp 197−231, Springer-Verlag, New York.
28. Mehler, E. L., Hassan, S. A., Kortagere, S., and Weinstein, H. (2006) *Ab initio* computational modeling of loops in G-protein-coupled receptors: Lessons from the crystal structure of rhodopsin. *Proteins 64*, 673–690.
29. Tartaglia, M., Mehler, E. L., Goldberg, R., Zampino, G., Brunner, H. G., Kremer, H., van der Burgt, I., Crosby, A. H., Ion, A., Jeffery, S., Kalidas, K., Patton, M. A., Kucherlapati, R. S., and Gelb, B. D. (2001) Mutations in PTPN11, encoding the protein tyrosine phosphatase SHP-2, cause Noonan syndrome. *Nat. Genet. 29*, 465–468.
30. Kortagere, S., Roy, A., and Mehler, E. L. (2006) Ab initio computational modeling of long loops in G-protein coupled receptors. *J. Comput.-Aided Mol. Des. 20*, 427–436.
31. Brooks, B. R., Brooks, C. L., III, Mackerell, A. D., Jr., Nilsson, L., Petrella, R. J., Roux, B., Won, Y., Archontis, G., Bartels, C., Boresch, S., Caflisch, A., Caves, L., Cui, Q., Dinner, A. R., Feig, M., Fischer, S., Gao, J., Hodoscek, M., Im, W., Kuczera, K., Lazaridis, T., Ma, J., Ovchinnikov, V., Paci, E., Pastor, R. W., Post, C. B., Pu, J. Z., Schaefer, M., Tidor, B., Venable, R. M., Woodcock, H. L., Wu, X., Yang, W., York, D. M., and Karplus, M. (2009) CHARMM: The biomolecular simulation program. *J. Comput. Chem. 30*, 1545–1614.
32. MacKerell, A. D., Jr., Bashford, D., Bellott, M., Dunbrack, R. L., Jr., Evanseck, J. D., Field, M. J., Fischer, S., Gao, J., Guo, H., Ha, S., Joseph-McCarthy, D., Kuchnir, L., Kuczera, K., Lau, F. T. K., Mattos, C., Michnick, S., Ngo, T., Nguyen, D. T., Prodhom, B., Reiher, W. E., III, Roux, B., Schlenkrich, M., Smith, J. C., Stote, R., Straub, J., Watanabe, M., Wiorkiewicz-Kuczera, J., Yin, D., and Karplus, M. (1998) All-Atom Empirical Potential for Molecular Modeling and Dynamics Studies of Proteins. *J. Phys. Chem. B 102*, 3586–3616.
33. Hassan, S. A., Guarnieri, F., and Mehler, E. L. (2000) A general treatment of solvent effects based on screened Coulomb potentials. *J. Phys. Chem. B 104*, 6478–6489.
34. Hassan, S. A., Mehler, E. L., Zhang, D., and Weinstein, H. (2003) Molecular dynamics simulations of peptides and proteins with a continuum electrostatic model based on screened Coulomb potentials. *Proteins 51*, 109–125.
35. Li, X. F., Hassan, S. A., and Mehler, E. L. (2005) Long dynamics simulations of proteins using atomistic force fields and continuum representation of solvent effects: Calculation of structure and dynamic properties. *Proteins 60*, 464–484.
36. Mehler, E. L. (1990) Comparison of dielectric response models for simulating electrostatic effects in proteins. *Protein Eng. 3*, 415–417.
37. Mehler, E. L., Fuxreiter, M., Simon, I., and Garcia-Moreno, E. B. (2002) The role of hydrophobic microenvironments in modulating pKa shifts in proteins. *Proteins 48*, 283–292.
38. Mehler, E. L., and Guarnieri, F. (1999) A Self-Consistent, Microenvironment Modulated Screened Coulomb Potential Approximation to Calculate pH Dependent Electrostatic Effects in Proteins. *Biophys. J. 77*, 3–22.
39. Mehler, E. L., and Warshel, A. (2000) Comment on "A Fast and Simple Method to Calculate Protonation States in Proteins. *Proteins: Struct., Funct., Genet. 40*, 1–3.
40. Noonan, J. A. (1968) Hypertelorism with Turner phenotype. A new syndrome with associated congenital heart disease. *Am. J. Dis. Child. 116*, 373–380.
41. Lee, K. A., Williams, B., Roza, K., Ferguson, H., David, K., Eddleman, K., Stone, J., Edelmann, L., Richard, G., Gelb, B. D., and Kornreich, R. (2009) PTPN11 analysis for the prenatal diagnosis of Noonan syndrome in fetuses with abnormal ultrasound findings. *Clin. Genet. 75*, 190–194.
42. Frishman, D., and Argos, P. (1995) Knowledge-based protein secondary structure assignment. *Proteins 23*, 566–579.
43. Roberts, E., Eargle, J., Wright, D., and Luthey-Schulten, Z. (2006) MultiSeq: Unifying sequence and structure data for evolutionary analysis. *BMC Bioinf. 7*, 382.
44. Warne, T., Serrano-Vega, M. J., Baker, J. G., Moukhametzianov, R., Edwards, P. C., Henderson, R., Leslie, A. G., Tate, C. G., and Schertler, G. F. (2008) Structure of a β_1-adrenergic G-protein-coupled receptor. *Nature 454*, 486–491.
45. Cherezov, V., Rosenbaum, D. M., Hanson, M. A., Rasmussen, S. G., Thian, F. S., Kobilka, T. S., Choi, H. J., Kuhn, P., Weis, W. I., Kobilka, B. K., and Stevens, R. C. (2007) High-resolution crystal structure of an engineered human β_2-adrenergic G protein-coupled receptor. *Science 318*, 1258–1265.

46. Sali, A., and Blundell, T. L. (1993) Comparative protein modelling by satisfaction of spatial restraints. *J. Mol. Biol. 234*, 779–815.
47. Okada, T., Sugihara, M., Bondar, A. N., Elstner, M., Entel, P., and Buss, V. (2004) The retinal conformation and its environment in rhodopsin in light of a new 2.2 Å crystal structure. *J. Mol. Biol. 342*, 571–583.
48. Kelley, L. A., Gardner, S. P., and Sutcliffe, M. J. (1996) An automated approach for clustering an ensemble of NMR-derived protein structures into conformationally related subfamilies. *Protein Eng. 9*, 1063–1065.
49. Canutescu, A. A., Shelenkov, A. A., and Dunbrack, R. L., Jr. (2003) A graph-theory algorithm for rapid protein side-chain prediction. *Protein Sci. 12*, 2001–2014.
50. Visiers, I., Ebersole, B. J., Dracheva, S., Ballesteros, J., Sealfon, S. C., and Weinstein, H. (2002) Structural motifs as functional microdomains in G-protein-coupled receptors: Energetic considerations in the mechanism of activation of the serotonin 5-HT2A receptor by disruption of the ionic lock of the arginine cage. *Int. J. Quantum Chem. 88*, 65–75.
51. Shan, J., Mehler, E. L., and Weinstein, H. (2009) Probing the Dynamic Structure and Function of Intracellular Loop 2 in Structurally Cognate GPCRs. *Biophys. J. 96*, 429a–430a.
52. Shan, J., Khelashvili, G., and Weinstein, H. (2010) Large-Scale MD Simulations Reveal Structural Elements of the Activated State in the 5-HT_{2A} Receptor and their Relation to Cholesterol Dynamics. *Biophys. J. 98*, 419a.
53. Aurora, R., and Rose, G. D. (1998) Helix capping. *Protein Sci. 7*, 21–38.
54. Dror, R. O., Arlow, D. H., Borhani, D. W., Jensen, M. Ã., Piana, S., and Shaw, D. E. (2009) Identification of two distinct inactive conformations of the β_2-adrenergic receptor reconciles structural and biochemical observations. *Proc. Natl. Acad. Sci. U.S.A. 106*, 4689–4694.
55. Ballesteros, J. A., Shi, L., and Javitch, J. A. (2001) Structural mimicry in G protein-coupled receptors: Implications of the high-resolution structure of rhodopsin for structure-function analysis of rhodopsin-like receptors. *Mol. Pharmacol. 60*, 1–19.